Deformation-induced phase transformations in the Al–Fe system under intensive plastic deformation

2007 J. Phys.: Condens. Matter 19 386222

(http://iopscience.iop.org/0953-8984/19/38/386222)

IOP PUBLISHING JOURNAL OF PHYSICS: CONDENSED MATTER

J. Phys.: Condens. Matter **19** (2007) 386222 (16pp) doi:10.1088/0953-8984/19/38/386222

Deformation-induced phase transformations in the Al–Fe system under intensive plastic deformation

V A Shabashov[1], I G Brodova, A G Mukoseev, V V Sagaradze and A V Litvinov

Institute of Metal Physics, Ural Branch RAS, Ekaterinburg, Russian Federation

E-mail: shabashov@imp.uran.ru

Received 27 December 2006, in final form 5 June 2007
Published 4 September 2007
Online at stacks.iop.org/JPhysCM/19/386222

Abstract

Mössbauer spectroscopy showed that mechanical activation by compression shear in Bridgman anvils led to deformation-induced dissolution of Al_6Fe and $Al_{13}Fe_4$ aluminides and iron in the aluminum matrix, which was followed by formation of an Al–Fe solid solution, Al_9Fe_2 and Al_5Fe_2 aluminides, and their defective modifications. The Al_6Fe and $Al_{13}Fe_4$ aluminides dissolved with an extraction-type stoichiometry, which was explained by an easier release of aluminum (as compared to iron) to the aluminum matrix and the accompanying precipitation of aluminides owing to saturation of the structure with deformation vacancies. A unified set of metastable phases, which appeared during quick quenching and intensive plastic deformation of the Al–Fe system, pointed to a common diffusion mechanism of the phase transformations.

1. Introduction

At present, researchers and engineers are paying much attention to dispersion-strengthened aluminum alloys. This also applies to the Al–Fe system, since iron is a natural impurity of aluminum and it forms a set of intermetallics even if its concentration in the aluminum matrix is small. Al–Fe alloys have been used in studies concerned with phase transformations and formation of solid solutions and intermetallic phases using quick quenching, mechanical synthesis (MS) and implantation of iron in aluminum. Those studies revealed metastable aluminide phases having different stoichiometry values, such as Al_mFe/Al_9Fe_2, Al_6Fe, Al_xFe, etc [1–9]. Superhigh quenching rates allowed forming Al–Fe solid solutions containing several per cent of iron [3, 9]. The alloy with 1 at.% Fe already had, apart from isolated Fe atoms, Al_mFe clusters. Mechanical activation of Al–Fe alloys in ball mills caused amorphization of Al_mFe clusters and additional supersaturation of the alloys with iron.

[1] Author to whom any correspondence should be addressed.

Our studies [10–14] demonstrated that solid solutions were formed more often under compression shear (CS) in Bridgman anvils than in ball mills. This is explained to some extent by a lower temperature of deformation [13]. An advantage of CS over mechanical activation in ball mills is invariability of the affected volume, in which it is possible to control the composition, temperature and the degree of deformation of the sample [10, 12]. Bulky (and not powdered) samples are deformed in a continuum. These factors provide extremely high degrees of true deformation and the switchover of the structure to the nanocrystalline or amorphous state. The control over the deformation temperature is especially important for elements forming interstitial solid solutions and metals having a high homologous temperature (including aluminum), in which diffusion of atoms and defects is facilitated. It was shown [10–12, 14] that the kinetics of the deformation-induced dissolution of secondary phases (carbides and oxides of iron) in metal matrices and the formation of solid solutions and secondary phases strongly depend on solubility of MS elements (carbon, oxygen and iron) and their thermodynamic activity in metal matrices. The solubility of aluminum and iron atoms in the aluminum matrix is largely different in the Al–Fe system. Furthermore, a high homologous temperature of aluminum and the opportunity to form metastable intermetallic phases with different stoichiometry values turn this system into a model for observation of the possible low-temperature deformation-induced migration of elements from intermetallics during their dissolution in the aluminum matrix and the formation of secondary phases.

The goal of this study was to analyze MS solid solutions of iron in aluminum and the dissolution mechanism of aluminides under CS at room temperature.

2. Materials and methods

Samples of bulky cast Al–2 mass% Fe and Al–5 mass% Fe alloys (hereinafter referred to as Al–2Fe and Al–5Fe, respectively) and a mixture of Al and Fe powders taken in the same proportions were subject to CS. Commercial Al and a superpure ^{57}Fe isotope were used for preparation of the Al–5Fe alloy and the powder mixtures. The Al–Fe alloys were crystallized from the melt under different cooling conditions: treatment 1—quick quenching (2×10^4 K s^{-1}); treatment 2—chill casting (100 K s^{-1}). The alloy structure (treatment 1) is shown in figure 1(*a*). It is seen that the alloy was crystallized following a metastable diagram with the formation of a quasi-eutectic. The composition of aluminides comprising the eutectic, which was determined by x-ray analysis, corresponded to stoichiometric Al_6Fe. The alloy (treatment 2) had a more equilibrium structure, which included primary $Al_{13}Fe_4$ aluminides and a eutectic formed by analogous aluminides and an aluminum-based solid solution (see figure 1(*b*). According to the x-ray analysis, the concentration of iron in the α solid solution was very small and the lattice spacing did not differ from the lattice spacing of pure aluminum. An $Al_{13}Fe_4$ sample with an ordered superstructure was used in the experiments in addition to the aforementioned systems. Bulky samples and powder mixtures were deformed intensively at 298 K by shear under a pressure of 6 GPa in Bridgman anvils, which were made of sintered WC, at a rate $\omega \sim 1$ rpm and a turning angle $n \times 2\pi$ ($n = 1$–20 being the number of turns) by the method described in [10–14]. In the CS method, the anvils are displaced radially because the structure is deformed in the bulk of the sample and the sample material does not exchange with the material of the anvils. The prepared sample was a bright disk 10 mm in diameter and about 80 μm thick. The disk was thinned on both sides to 30 μm for the Mössbauer analysis. The true deformation was estimated from the formula $\varepsilon = \ln(\varphi r/d)$, where φ is the turning angle, r is the radius (the middle of the peripheral region under study), and d is the thickness of the deformed sample. The anvils were turned through 1–20 revolutions, which corresponded to the true deformation $\varepsilon = 4$–8. The Mössbauer spectra were measured in the geometry for

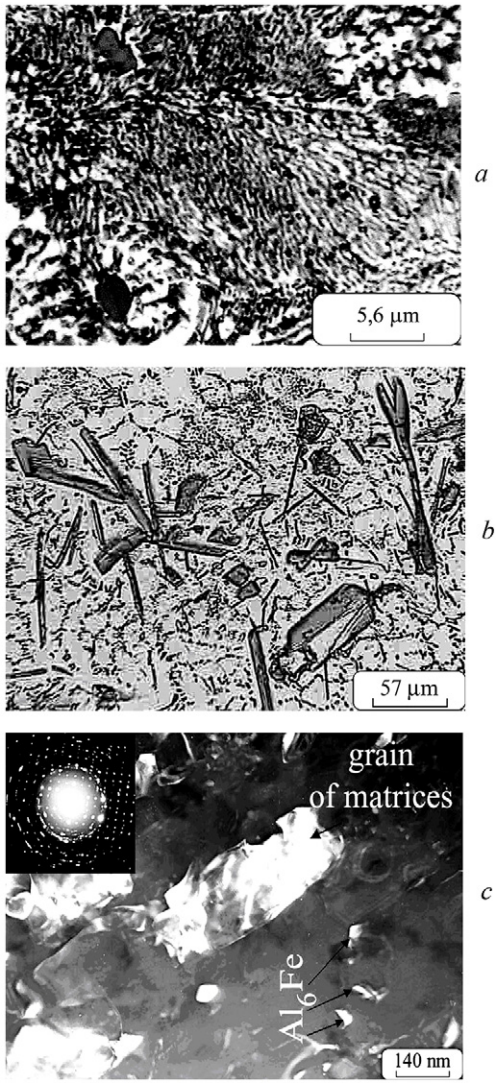

Figure 1. Microstructure of the Al–5Fe alloy. Treatment: (*a*) quick quenching; (*b*) chill casting; (*c*) CS ($n = 5$) of the quickly quenched alloy (a dark-field image and an electron diffraction pattern of the alloy structure).

transmission of 14.4 keV gamma-quanta from a ^{57}Co(Rh) source under a constant acceleration regime. The microstructure was examined in a JEM-200CX transmission electron microscope. The x-ray diffraction analysis (XDA) was performed using a DRON-4-07 diffractometer with copper irradiation. The local composition of the intermetallics was determined using x-ray spectral analysis in a Jeol 840 scanning electron microscope (SEM).

A special software package, MS Tools [15], providing reconstruction of the density function of Mössbauer spectra, was used to improve the Mössbauer spectrum resolution. The density function of the centers of gravity of the resonance absorption lines, $P(V)$, on the Doppler velocity scale was reconstructed without establishing any *a priori* correlations between the Mössbauer parameters. Then the $P(V)$ function was approximated by a linear

Table 1. Mössbauer parameters of phases in the Al–5Fe and Al–2Fe alloys (relative to αFe).

	Metastable phases							Stable phases		
Parameter	Al–Fe	Al–Fe(d)	Al_6Fe	Al_6Fe(d)	Al_9Fe_2	Al_9Fe_2(d)	Al_iFe	$Al_{13}Fe_4$		Al_5Fe_2
I_S (mm s^{-1})	0.42	0.18–0.20	0.23	0.20	0.12	0.06	0.36	0.202	0.201	0.24
ΔQ_S (mm s^{-1})	—	—	0.32	0.38	0.32	0.60	0.56	—	0.38	0.46

combination of modified Gaussian lines to determine individual distributions corresponding to positions of iron in the oxides and the alloys. Considering a diversity of aluminide phases, possible distortions caused by deformation defects and nonstoichiometry, and a complexity involved in the correlation of the Mössbauer parameters (the isomer shift I_S, the quadrupole splitting Q_S, and the integral intensity S), this calculation procedure is most efficient for both an independent evaluation of the phase composition and subsequent modeling on the basis of a standard approximation of the spectra by a superposition of Lorentzian absorption lines.

3. Results

3.1. Dissolution of Al_6Fe aluminide in Al–2Fe and Al–5Fe alloys

Almost all iron in the Al–5Fe alloy having the structure of a metastable quasi-eutectic, which was prepared by quick quenching of the melt (treatment 1), was bound to metastable Al_6Fe. This conclusion followed from analysis of the spectrum, which was described by a symmetric doublet [2–4]; see figure 2(*a*). However, already after quenching some iron might be found in the metastable Al_9Fe_2/Al_mFe aluminide; see figure 2(*b*). After the Al–5Fe alloy was deformed by compression shear at 6 GPa with $n = 10$ and 20, its spectrum had an additional line with parameters of a solid solution of iron in the aluminum matrix (Al–Fe) and the doublet of the metastable Al_9Fe_2 phase appeared and built up in the spectrum. Lines of the initial Al_6Fe doublet shifted to positions of the Al_6Fe(d) doublet having similar, but largely different, Mössbauer parameters (see figures 2(*c*), (*d*) and table 1), which coincided with those of the main doublet of the $Al_{13}Fe_4$ structure. Some amount of the structure described by the Al_6Fe(d) doublet could be also formed in the Al–5Fe alloy after quenching (figure 2(*b*)).

Along with the doublet of metastable Al_6Fe, the Al_9Fe_2 phase and an additional Al_6Fe(d) doublet were observed in the spectrum of the less concentrated Al–2Fe alloy already after its quenching (figure 3(*a*)). In the spectrum of the Al–2Fe alloy, which was deformed at $n = 1$ and 3, the Al_6Fe and Al_9Fe_2 doublets partially turned to the line (the singlet) of the Al–Fe solid solution and the Al_6Fe(d) and Al_9Fe_2(d) doublets (figure 3(*b*)). The singlet of the Al–Fe solid solution stood out well in the alloys already at $n = 1$–3 and its surface area expanded as the degree of deformation increased up to $n = 10$ and 20.

Thus, taking two different alloys, Al–5Fe and Al–2Fe, as an example, it was demonstrated that the Al_6Fe(d) and Al_9Fe_2 doublets were present in the spectra of these two alloys often immediately after quick quenching of the alloys (treatment 1). The Al_9Fe_2 structure was observed earlier in experiments on quenching at rates of over 2×10^4 K s^{-1} and was assumed to be a metastable phase with a body-centered (BC) tetragonal lattice [9]. The formation of the modified Al_6Fe(d) structure after quenching probably could be explained by saturation of the structure with defects like vacancies owing to large temperature gradients and mechanical stresses arising upon quick cooling.

The established fact that the isomer shift diminishes on transition from the line of the Al–Fe solid solution to its defective modification in the form of aluminum vacancies near

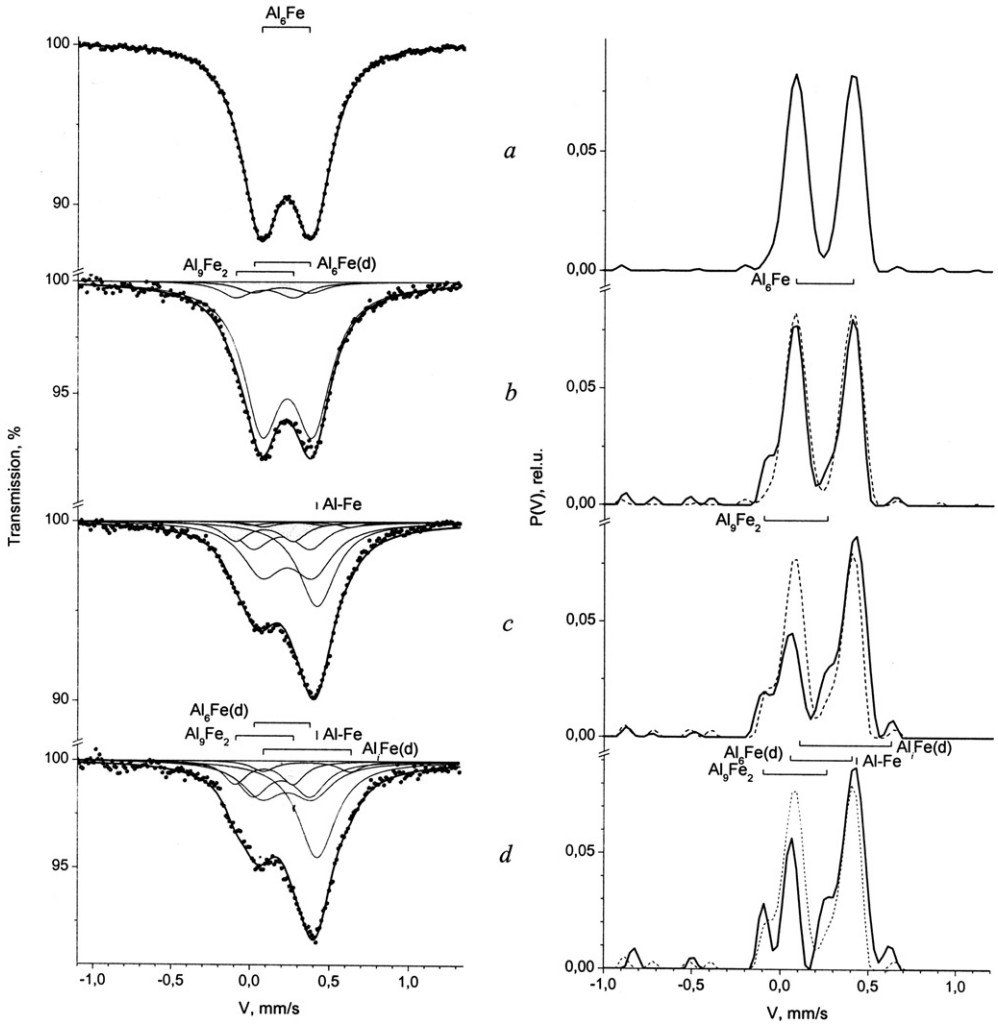

Figure 2. Mössbauer spectra and $P(V)$ functions of the Al–5Fe alloy. Treatment: (*a*) and (*b*) quick quenching (treatment 1); (*c*) treatment 1 + shear ($n = 10$), (*d*) treatment 1 + shear ($n = 20$). The Al–5Fe was smelted with 5 wt% of ^{57}Fe.

iron atoms in Al–Fe(d) [5–8] and from Al_6Fe to Al_9Fe_2 [3, 4] (that is, the Al concentration of the aluminide decreased) reflected the predominant effect of the 3d–3p electron exchange and the decrease in electronegativity of iron with decreasing aluminum concentration. It is reasonable to assume therefore that the Al_6Fe(d) and Al_9Fe_2(d) modifications (similarly to metastable Al_9Fe_2), whose isomer shifts are negative relative to the isomer shift of Al_6Fe, appeared when aluminum atoms passed to the matrix. They may be conditionally viewed as structures of the $Al_{6-x}Fe$ and $Al_{9-x}Fe$ types, that is, with a subtraction-like stoichiometry. If the iron concentration of the aluminides ($Al_{13}Fe_4$, Al_5Fe_2, etc) rises, the dependence of I_S on the composition becomes more complicated probably due to a mutual effect of the electronic structures of iron atoms [16]. Larger Q_S of the Al_6Fe(d) and Al_9Fe_2(d) doublets than those of the doublets of the initial phases is explained by the increase in the defect content of the lattice in the newly formed aluminides. Deformation-induced Al_6Fe(d) and Al_9Fe_2(d) structures were

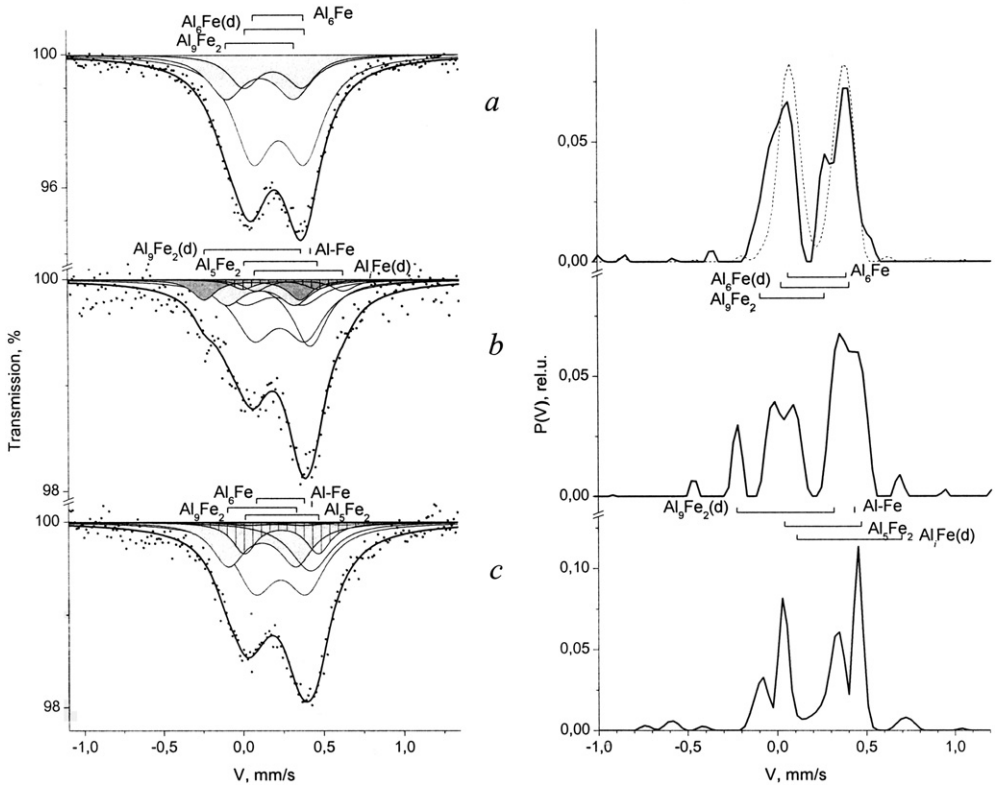

Figure 3. Mössbauer spectra and $P(V)$ functions of the Al–2Fe alloy. Treatment: (*a*) quick quenching (treatment 1); (*b*) treatment 1 + shear ($n = 3$); (*c*) treatment 1 + shear ($n = 3$) + annealing, 473 K, 20 min. The Al–2Fe alloy was smelted with 2 wt% of natural Fe.

extremely unstable. This was confirmed by the experiment on low-temperature annealing at 473 K (20 min), which led to a partial 'recovery' of the spectra, that is, the changeover of the $Al_6Fe(d)$ and $Al_9Fe_2(d)$ doublets and, also, the singlet of the Al–Fe solid solution to doublets of Al_9Fe_2 and Al_6Fe (see figure 3(*c*)). Thermal and mechanical instability of $Al_6Fe(d)$ and, similarly, of $Al_9Fe_2(d)$ confirms the vacancy origin of defects in these structural components. The assumption on structural vacancies in the aluminides is supported by experiments, which were performed by Preston *et al*, on implantation of iron in aluminum, quick quenching, and cold deformation of dilute Al–Fe alloys [5–8]. The wide lines of Al–Fe(d), which were shifted to the region of negative rates with respect to the line of the Al–Fe solid solution, were related [5, 6] to 0, 1, 2, ... vacancies of aluminum atoms near an iron atom.

The XDA and TEM examinations of the same samples of the Al–5Fe and Al–2Fe alloys (see below and [17]) revealed the presence of the α solid solution and metastable Al_6Fe aluminides. Since Mössbauer spectroscopy allows analysis of the structure at the level of nearest atomic neighbors, the formation of the singlet of the iron-supersaturated solid solution and doublets nonequivalent to the initial Al_6Fe might point to the disturbance of the short-range atomic order in Al_6Fe and saturation of the aluminides with structural vacancies by subtraction like $Al_{6-x}Fe$.

The metastable structure with the Al_5Fe stoichiometry, which was detected in [9], is of interest if one considers that the $Al_6Fe(d)$ doublet was formed already during quick quenching

Table 2. Treatment and phase composition (S, %) of Al–5 mass% Fe and Al–2 mass% Fe alloys and a powder mixture of Al–5 mass% Fe in the initial state (treatments 1 and 2 and powder mixtures), after shear n at a pressure of 6 GPa, and after annealing at 473 K for 20 min.

	Alloy								Mixture		
	Al–5Fe					Al–2Fe			Al–5Fe[a]		
Phase composition (+5%)	Treat 1	Shear $n = 10$	Shear $n = 20$	Treat 2	Shear $n = 10$	Treat 1	Shear $n = 3$	Annealing	Initial	Shear $n = 10$	Annealing
Al_6Fe	86	39	27	36	10	60	35	43	—	—	30
Al_6Fe(d)	8	16	21	24	15	15	15	2	—	32	—
Al_9Fe_2	6	10	11	—	8	24	13	23	—	20	11
Al_9Fe_2(d)	—	—	—	—	8	—	8	—	—	8	—
Al_3Fe	—	—	—	40	34	—	—	—	—	—	—
Al_5Fe_2	—	—	—	—	9	—	4	13	—	12	46
Al–Fe	—	31	36	—	11	—	20	17	—	18	13
Al_iFe(d)	—	3	5	—	5	—	5	2	—	10	—

[a] For the Al–5Fe alloy prepared by mechanical synthesis from a powder mixture the table gives the relative concentration of iron-containing phases, which were described by the central (non-Zeeman) portion of the spectrum accounting for 14%. The rest corresponded to the sextet of ferromagnetic αFe.

and its amount increased after deformation. This structure was formed in a similar alloy, which was cooled at a rate of 0.5–5 $\times$ 10^3 K s^{-1}, but the type of its crystal lattice was not identified reliably. It may be thought that the metastable Al_6Fe(d) structure, which was formed during quenching and deformation, and the phase [9] have a similar stoichiometry. This supposition is supported additionally by the overlap of the quenching rate intervals of Al_5Fe, Al_6Fe [9] and detected Al_6Fe(d).

The number of nonequivalent neighbors of iron atoms represented by Al_6Fe(d) may grow (see curves (*a*) and (*b*) in figure 2 and table 2) and reach 10% or more after deformation. The formation of such an insignificant amount of the Al_6Fe(d) structure after quenching or intensive deformation on the assumption of one aluminum vacancy per formula unit of Al_6Fe, i.e. on the assumption of the Al_5Fe stoichiometry, may suggest a concentration of structural vacancies equal to 2–3%. This estimate disregards the position of vacancies in the aluminide structure and assumes the predominant effect of the aluminide stoichiometry on the Mössbauer parameters.

Thus, Al_6Fe and Al_9Fe_2 aluminides and dilute Al–Fe [6] solid solutions may form during deformation of their defective modifications Al_6Fe(d), Al_9Fe_2(d) and Al–Fe(d) as a result of saturation with structural vacancies. Ratios of the isomer shifts of the metastable phases and their modifications are given in table 1.

In addition to the aforementioned components, deformed Al–5Fe and Al–2Fe alloys formed the Al_iFe(d) doublet with wide lines (see figures 2(*c*), (*d*) and 3(*b*)), which was shifted to the region of positive rates relative to the initial Al_6Fe doublet. The former doublet may result from a superposition of several doublets with similar parameters. The Al_iFe(d) doublet cannot be interpreted *a priori* using Mössbauer data. The spectrum of the Al_5Fe_2 aluminide, which in our case results from dissolution of Al_6Fe in the aluminum matrix, may contribute to the wide doublet (see tables 1 and 2). The integral intensity of the Al_iFe(d) doublet was within the experimental error. In what follows we shall substantiate the necessity to distinguish between the Al_iFe(d) and Al_5Fe_2 doublets. The annealing experiment demonstrated that the Al_iFe(d) doublet had a low thermal stability (see figure 3(*c*)), i.e. it was related probably to point defects, composition inhomogeneities or nonequilibrium boundaries of dispersed aluminides, which

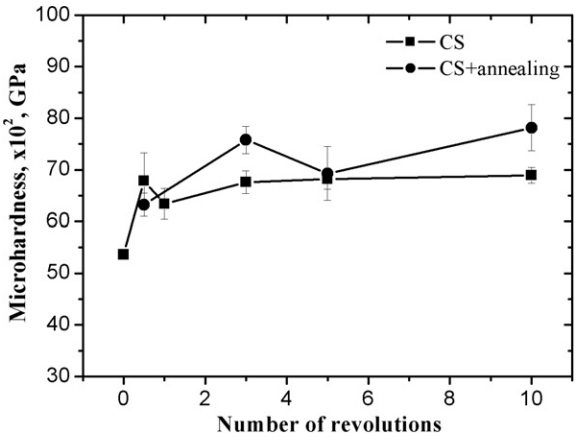

Figure 4. Variation of the lattice spacing and microstresses of the α solid solution in the Al–2Fe alloy depending on the degree of deformation.

transformed during recovery. The Al_iFe(d) doublet transformed to the Al_5Fe_2 doublet upon annealing.

Thus, the analysis of the Mössbauer spectra revealed that deformation of the quasi-eutectic structure containing metastable Al_6Fe aluminides led to their partial dissolution, which caused the deformation-induced formation of a supersaturated solid solution of iron in aluminum and metastable Al_9Fe_2 aluminides. Moreover, it was shown that these phases had a defective structure resulting from accumulation of point defects during CS cold deformation.

The results of the Mössbauer spectroscopy were verified using data obtained by other methods, specifically TEM and XDA [17–19].

According to the XDA, different degrees of deformation ($n = 1$–5) led to a decrease in the lattice parameter of the α solid solution, a fact which confirmed the Mössbauer data pointing to additional supersaturation of the matrix with iron. The variation of the lattice parameter of the α solid solution in Al–2Fe depending on the degree of deformation is shown in figure 4. The maximum concentration of Fe in the α solid solution was not over 1.2% in Al–2Fe and 1.5% in Al–5Fe under the given deformation conditions.

Figure 1(*c*) illustrates the variation of the structure of the quasi-eutectic compound during CS. According to the TEM data, a submicrocrystalline structure with grains 150 to 200 nm in size was formed. Grain boundaries were smeared and were not clearly discriminated. A nonuniform contrast testifying to a strong cold work hardening of the material was observed in the matrix grains. The evaluation of microstresses in the matrix lattice, which was done by analyzing widening of the physical line $(311)_\alpha$, showed variation of the microstressed state with increasing n (figure 4). Taking the Al–2Fe alloy as an example, it is seen that the defect content of the structure, which was responsible for deformation strengthening, sharply increased already at small degrees of deformation. The largest number of defects was concentrated at the matrix–aluminide interface. The iron aluminides were fragmented, decomposed and dissolved partially in the aluminum matrix during deformation. At $n = 5$ the crystals were as large as 10 nm. The dark-field image in the coinciding reflection of the aluminum matrix and the Al_6Fe aluminide shows the dimensional scale of the two phases. The defect structure of the aluminides could be judged by the nonuniform contrast and appearance of subgrains in the crystals. These results validated the conclusions of the Mössbauer spectroscopy that additional spectra of deformation modifications Al_6Fe(d), Al_9Fe_2(d) and Al_iFe(d) appeared during deformation.

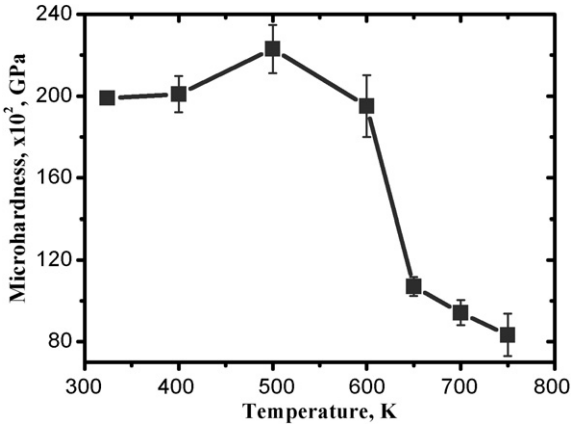

Figure 5. Microhardness of the Al–2Fe alloy after CS ($n = 5$) and subsequent isochronal (30 min) annealing.

In addition to the Mössbauer spectroscopy and XDA methods, the intermetallics were identified by their chemical composition using the local x-ray spectrum analysis in a Jeol 840 SEM rated at 10 kV and outfitted with an energy dispersion spectroscopy attachment (EDS Link-Oxford). The analysis of the chemical composition showed that after CS Al_6Fe crystals co-existed with aluminides containing 78.36 at.% Al, 18.87 at.% Fe and 2.77 at.% O, i.e. $Al_{8.5}Fe_2$. This observation confirmed the possibility of the deformation-induced transformation of the metastable Al_6Fe phase to Al_9Fe_2 and the appearance of intermediate deformation structures like Al_6Fe(d) and Al_9Fe_2(d) having a nonstoichiometric composition.

To check the thermal stability of the mechanically synthesized samples, their matrix lattice parameter, microhardness and microstresses of the II kind were measured and the TEM study was performed after the samples were annealed at a temperature from 373 to 773 K. It was concluded that recovery processes were active in the deformed material over the interval from room temperature to 600 K. They were accompanied by the decrease in microhardness and microdistortions of the matrix lattice and the appearance of more equilibrium grain boundaries with a banded contrast. The grain size remained virtually unchanged and did not exceed 200 nm. At 473 K the $H_v = f(T)$ dependence exhibited a maximum (figure 5), which could be due, considering the decrease of this parameter with heating, only to dispersion hardening, i.e. decomposition of the supersaturated solid solution. Although the annealing time was short (0.5–1 h), an examination of the dark-field image (in the reflection of the metastable Al_6Fe aluminide) of the sample, which was deformed by shear at $n = 5$ turns, revealed initial stages of decomposition in the form of fine precipitates at boundaries and in the bulk of grains. These results support the Mössbauer spectroscopy data indicating that the spectrum component related to the supersaturated solid solution decreased and the Al_6Fe and Al_9Fe_2 components increased upon heating up to 473 K. Moreover, the spectrum components, which characterized defect states of structural components Al_6Fe(d), Al_9Fe_2(d) and Al_iFe(d), became much less intense. The components Al_6Fe and Al_9Fe_2 increased.

3.2. Dissolution of the $Al_{13}Fe_4$ aluminide in the Al–5Fe alloy

The Mössbauer spectrum of the alloy, which was prepared by the treatment 2, was a superposition of the spectra of the $Al_{13}Fe_4$ superstructure (the doublet and the central line)

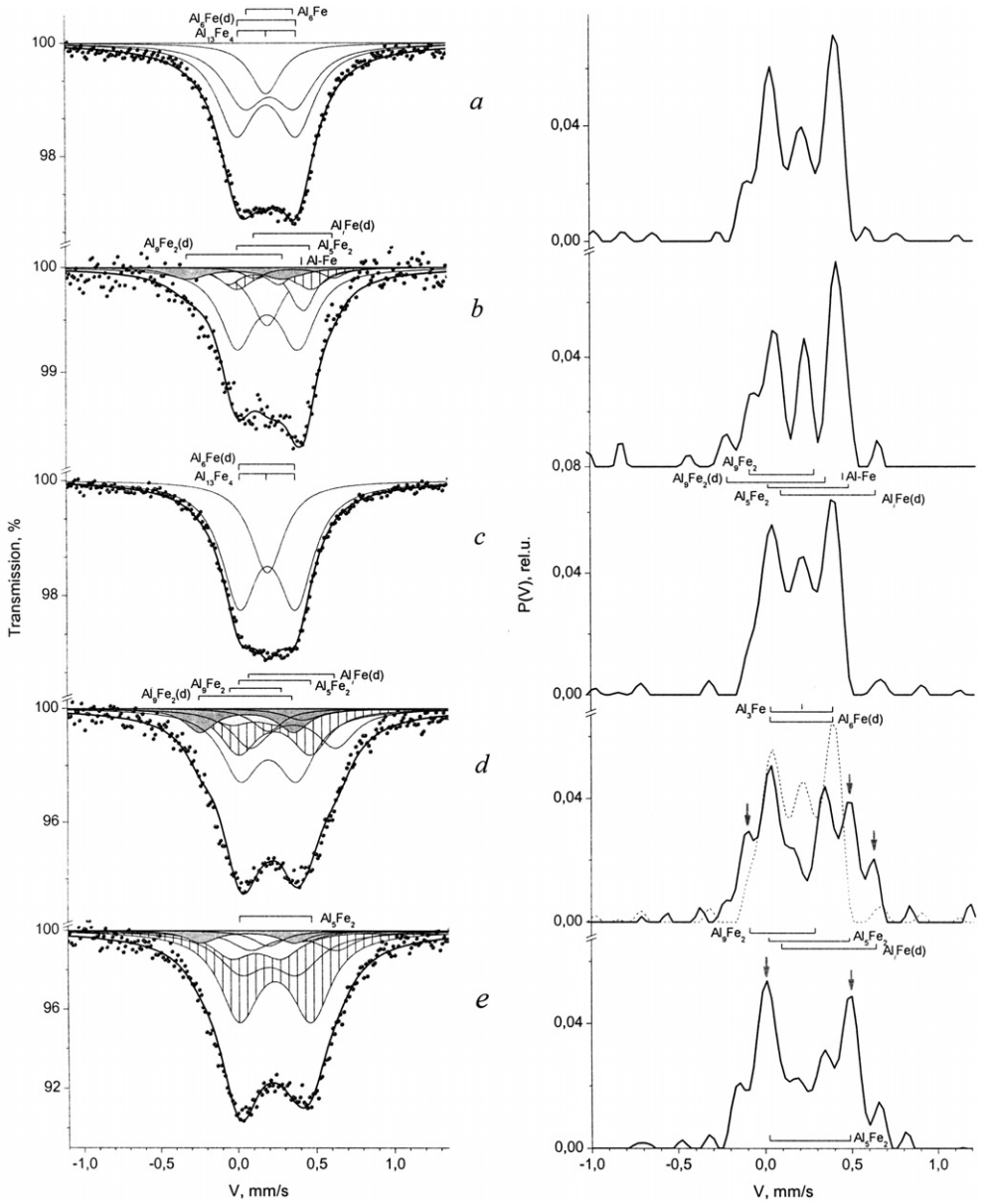

Figure 6. Mössbauer spectra and $P(V)$ functions of the Al–5Fe ((*a*), (*b*)) and $Al_{13}Fe_4$ ((*c*)–(*e*)) alloys. Treatment: (*a*) chill casting (treatment 2); (*b*) treatment 2 + shear ($n = 5$); (*c*) casting; (*d*) casting + shear ($n = 5$); (*e*) casting + shear ($n = 5$) + holding two weeks at room temperature.

and the Al_6Fe and Al_9Fe_2 doublets (see figure 6(*a*)). The presence of metastable aluminides (Al_6Fe and Al_9Fe_2) after treatment 2 was due to a nonuniform cooling rate of the sample's volume during chill casting and the formation of the metastable Al–Al_6Fe eutectic. The latter amounted to 30%, as can be seen from table 2.

The subsequent shear deformation ($n = 5$ at 6 GPa) led to the formation of a relatively small amount of the Al–Fe solid solution (figure 6(*b*)). The concentration of the basic structure

$Al_{13}Fe_4$ did not change and the Al_6Fe spectrum component changed most. In accordance with the results given in section 3.1, it is this phase that experienced structural transformations during deformation. Similarly to section 3.1, the change of the spectrum shows up as the increase in the contribution from the defective modifications, which are characteristic of deformation of quickly quenched alloys.

A more intensive treatment ($n = 10$ and $P = 6$ GPa) caused an insignificant additional growth of the Al–Fe line. The spectrum intensity of the $Al_{13}Fe_4$ component decreased a little.

Thus, the interpretation of the spectrum of the Al–5Fe alloy containing the $Al_{13}Fe_4$ aluminide (treatment 2) showed that high degrees of deformation ($n = 10$ and $P = 6$ GPa) led to the formation of an inconsiderable amount of the Al–Fe solid solution and phase modifications, which appeared, thanks to the deformation dissolution of Al_6Fe aluminides in the aluminum matrix. The dissolution kinetics of the $Al_{13}Fe_4$ aluminide after treatment 2, which was followed by the formation of a solid solution and defective modifications, was much inferior to the dissolution kinetics of the Al_6Fe aluminide. The concentration of Al_9Fe_2 and Al_9Fe_2(d) increased and an insignificant amount of the structure with parameters of Al_5Fe_2 and Al_iFe(d) appeared in the spectrum with growing degree of deformation. The spectrum of deformed $Al_{13}Fe_4$ will be analyzed in more detail in section 3.3.

In order to establish the mechanism of the phase transformations and, in particular, ascertain the role of the aluminum matrix in the formation of new solid solutions and phases, it was reasonable to perform experiments on the deformation-induced synthesis of aluminum and iron powders and CS deformation of the $Al_{13}Fe_4$ superstructure without the aluminum matrix.

3.3. Compression shear of the $Al_{13}Fe_4$ structure

In contrast to the experiments described above, the $Al_{13}Fe_4$ superstructure was deformed in the absence of aluminum. Therefore, it was possible to analyze deformation transformations in $Al_{13}Fe_4$ excluding the possible transfer of aluminum or iron atoms out of the aluminide. A detailed description of the spectrum (figures 6(*c*) and (*d*)) demonstrated that the initial $Al_{13}Fe_4$ triplet diminished and the Al–Fe singlet was absent after deformation, while doublets (namely Al_9Fe_2, Al_5Fe_2 and Al_iFe(d)), which were observed in the experiments on dissolution of the Al_6Fe and $Al_{13}Fe_4$ aluminides in aluminum, were formed.

In accordance with the presumed stoichiometry, partial contributions (in terms of iron) of the newly formed components followed the balance equation

$$1(Al_{3.2}Fe) \cong 0.11(Al_9Fe_2) + 0.27(Al_{3.2}Fe) + 0.13(Al_5Fe_2) + 0.12(Al_iFe(d)). \quad (1)$$

Equation (1) shows that the stoichiometry of the Al_iFe(d) component approached the stoichiometry of Al_5Fe_2. Long holding at room temperature or heating to 470 K for 20 min led to an increase in the Al_5Fe_2 doublet at the expense of deformation-induced Al_iFe(d); see figure 6(*e*).

XDA confirmed the formation of the Al_5Fe_2 aluminide (figure 7). The x-ray photograph of the initial sample contained a set of narrow x-ray peaks corresponding to known tabulated data for the $Al_{13}Fe_4$ phase with the *R3m* rhombohedral lattice. The diffraction pattern of the deformed sample comprised a superposition of two x-ray photographs of the $Al_{13}Fe_4$ and Al_5Fe_2 phases having the *Cmcm* orthorhombic lattice and the parameters $a = 7.65$, $b = 7.41$ and $c = 4.22$ Å. The latter phase was consistently reproduced in the experiments. The observed strong smearing of the x-ray peaks at the Wolf–Bragg angles $2\theta = 15°$–$25°$ suggested the formation of very dispersed phases whose stoichiometry approached the stoichiometry of the $Al_{13}Fe_4$ and Al_5Fe_2 aluminides.

The change of the $Al_{13}Fe_4$ superstructure, which contained about 100 atoms in a unit cell [20], was probably due to deformation disordering and structural transformations, which

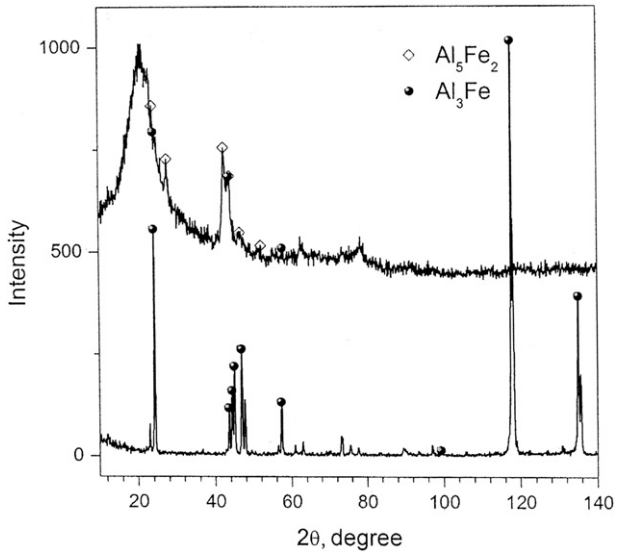

Figure 7. X-ray photograph of cast-recrystallized $Al_{13}Fe_4$ after CS ($n = 5$) deformation + holding two weeks at room temperature. Given below is a diffraction pattern of the $Al_{13}Fe_4$ structure.

could lead to the appearance of solid solutions with a random distribution of atoms. Stochastic processes of atomic distribution most probably resulted in compositions with a high or low concentration of aluminum, but approaching $Al_{13}Fe_4$. This deformation-induced nearly stochastic distribution of iron atoms in the $Al_{3.2}Fe$ structure might lead to the formation of solid solutions and pre-precipitates at the level of nearest neighbors with compositions similar to known phases, such as Al_9Fe_2, Al_5Fe_2, $Al_{13}Fe_4$, etc. It may be assumed that the newly formed components in the spectra corresponded to fore-precipitates of intermetallic phases. According to the Mössbauer data, partial contributions of iron to the formed phases were close to those described by a stochastic distribution. This distribution can arise in the structure of a solid solution having an order of the cluster short-range type [21]. The formation of the Al_5Fe_2 structure from $Al_{13}Fe_4$ reflected the realization of solid-state reactions involving the appearance of a stable aluminide with a simpler crystal lattice.

The experiment on deformation of the stable $Al_{13}Fe_4$ aluminide without the aluminum matrix demonstrated that dissolution of $Al_{13}Fe_4$ could differ from dissolution of metastable Al_6Fe. That is, it could involve disordering, formation of a solid solution, and then appearance of defective aluminides. Higher stability of the $Al_{13}Fe_4$ structure as compared to metastable Al_6Fe and Al_9Fe_2 under CS probably was explained by the additional energy consumption for disordering of this structure and the formation of the solid solution.

3.4. Synthesis of the Al–5Fe powder mixture

The analysis of spectra of the samples, which were prepared by CS ($n = 10$ and $P = 6$ GPa) of a powder mixture of Al and 5 mass% ^{57}Fe, showed that only a small portion of iron (about 0.7%) participated in the mechanical synthesis. Out of the 0.7%, 0.15% iron passed to the aluminum matrix at $n = 10$ and formed the singlet of the Al–Fe solid solution (see figure 8(*a*)). Similarly to deformation of the sample containing Al_6Fe (treatment 1), this structural component increased with the degree of deformation (see figure 8(*c*)). Along with the

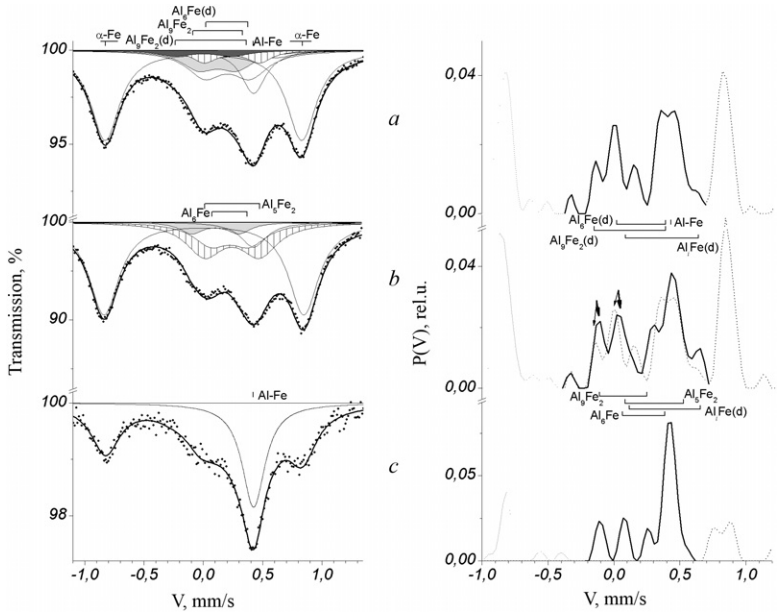

Figure 8. Mössbauer spectra and $P(V)$ functions of the Al–5Fe powder mixture. Treatment: (*a*) shear ($n = 10$); (*b*) shear ($n = 10$) + annealing (473 K, 20 min), (*c*) shear ($n = 20$).

Al–Fe component, the spectra contained lines of metastable Al_9Fe_2 and defective modifications $Al_6Fe(d)$, $Al_9Fe_2(d)$ and $Al_iFe(d)$. These doublets were resolved most clearly in spectra of samples synthesized from the powder mixtures. This fact was explained by the absence of the superposition of spectra of other aluminides because their concentration was small. It is remarkable that aluminum did not pass to iron during deformation, a feature which is characteristic of the initial stage of mechanical synthesis of metals having largely different hardness values and melting temperatures. Since the Al–Fe singlet and the $Al_iFe(d)$, $Al_6Fe(d)$ and $Al_9Fe_2(d)$ doublets were sensitive to temperature, they transformed to Al_5Fe_2, Al_6Fe and Al_9Fe_2 during annealing at 473 K for 20 min (see figure 8(*b*)).

The samples, which were prepared from powder mixtures by CS, contained large volumes of a supersaturated Al–Fe solid solution and defective modifications $Al_6Fe(d)$ and $Al_9Fe_2(d)$ as compared with volumes of metastable Al_6Fe and Al_9Fe_2. One may think therefore that the Al–Fe solid solution and defective $Al_6Fe(d)$ and $Al_9Fe_2(d)$ phases were intermediate in the formation of known aluminides.

4. Discussion

The observed dissolution of metastable Al_6Fe can be interpreted using ideas about the mechanism of mechanical synthesis with a 'subtraction'-type variation of the aluminide stoichiometry when Al_6Fe aluminides release predominantly aluminum atoms to the aluminum matrix during dissolution. Deformation-induced dissolution provides conditions for the formation, on the one hand, of iron-supersaturated solid solutions and, on the other hand, of metastable aluminides with a low aluminum content. In this case, phase transformations involving deformation dissolution of aluminides in the aluminum matrix can be written as

$$Al_6Fe + Al \rightarrow Al_{6-x}Fe + Al\text{–}Fe + Al. \quad (2)$$

The usual diffusion of substitutional atoms in alloys at room temperature does not take place even in the stress field of dislocations [22]. Vacancies and interstitial atoms, which are generated by cold deformation (at 298 K), sharply activate processes of decomposition and transport of aluminide atoms to the surrounding metal matrix [13, 22]. Refinement of the structure, its saturation with defects, a high homologous temperature of aluminum and poor solubility of iron provide conditions for phase transformations, which are followed by the change of the aluminide stoichiometry and appearance of supersaturated solid solutions. The formation of the defective modification Al_6Fe(d) and metastable Al_9Fe_2, which takes place both during quick quenching and severe plastic deformation, points to a common diffusion mechanism of phase transformations in the structure under these conditions. In the case of deformation dissolution of the aluminides, the variance of their Mössbauer parameters increases due to the generation of structural vacancies and appearance of Al_6Fe(d), Al_9Fe_2(d) and Al_iFe(d) phases. The saturation with vacancies may lead in the limiting case to amorphization of the structure [1, 2].

A reason for the predominant transport of aluminum from the aluminides to the aluminum matrix may be a high probability of aluminum atoms (especially in Al_6Fe) meeting deformation-induced vacancies and dislocations, which participate in processes of the atomic mass transfer. Metastable Al_6Fe(d) and Al_9Fe_2(d) phases, which are formed under intensive cold plastic deformation, may be caused by saturation of the initial metastable Al_6Fe and Al_9Fe_2 phases with structural vacancies owing to the release of aluminum atoms to the aluminum matrix and subsequent phase transformations. When the structure is saturated with deformation vacancies, the newly formed defective aluminides and supersaturated solid solutions can transform to other phases having the subtraction-type stoichiometry. This may be the reason for the formation of the Al_9Fe_2 phase from the higher metastable Al_6Fe aluminide.

Reverse transformations take place simultaneously by the scheme

$$Al_6Fe(d) \rightarrow Al_6Fe, \tag{3}$$

$$Al_9Fe_2(d) \rightarrow Al_9Fe_2, \tag{4}$$

which is realized thanks to nonequilibrium vacancies and is confirmed in experiments on low-temperature annealing of deformed samples. Notice that annealing of deformed Al–2Fe and Al–5Fe changed little the amount of the solid solution described by the Al–Fe singlet. This observation confirmed the predominant participation of the defective aluminides in the structural transformations.

One more reason, and, probably, the main reason for the predominant release of aluminum atoms from aluminides as compared to iron atoms, is the high energy and poor solubility of iron atoms in aluminum [2]. A regular feature that the concentration of the less soluble and less diffusive mobile element (iron in our case) increases in the formed dispersed phase was confirmed. A similar deformation-induced selective release was observed, for example, for dissolution of iron oxides in metal matrices, which caused a nonstoichiometry and its growth in the structure of the $Fe_{3-v}O_4$ inverse spinel [11, 12]. Cation-deficient oxides are formed, thanks to the higher (as compared to oxygen) solubility of iron in metal matrices. Note that the kinetics of deformation-induced dissolution depends on solubility and reactivity of oxide components (iron and oxygen) in metal matrices. One more example is dissolution of the Fe_3C cementite in iron, which is followed by the formation of metastable Fe_2C and Fe_5C_2 carbides with a low iron concentration [10, 12]. Considering the results of the deformation-induced transformation [10], the first stage of dissolution can be presented as the scheme $Fe_3C \rightarrow$ Fe–C+clusters Fe_4C [23]. At this stage, carbon is removed predominantly from the cementite. Secondary metastable ε and χ carbides appear from the carbon-supersaturated deformation-induced Fe–C solid solution.

By analogy with the above discussion, one may think that supersaturated Al–Fe solid solutions also may present a source for the formation of aluminides during CS of mixtures. This assumption is confirmed by deformation of the Al + 5 mass% Fe mixture, in which the singlet of the supersaturated Al–Fe solid solution considerably decreased upon annealing (figure 8). The observed phase transformations are undoubtedly determined by a high homologous temperature of aluminum and depend on experimental conditions (the pressure, the rate and temperature of deformation, etc), which control competitive processes of dynamic dissolution and precipitation of phases. Metastable nonstoichiometric aluminides may be formed due to local saturation of aluminum with iron by the mechanism of deformation-induced flows of nonequilibrium vacancies [24] or the lattice interstitial diffusion [22, 25], which are in dynamic equilibrium with processes of equilibrium precipitation of the phases.

The experiments with $Al_{13}Fe_4$ without the aluminum matrix demonstrated that the mechanism of dissolution of this structure in the aluminum matrix may be more complicated. It may involve disordering and appearance of supersaturated solid solutions, and then, at the level of nearest atomic neighbors, the formation of metastable aluminides and their defective modifications having similar compositions when the stoichiometry changes towards a higher or lower concentration of aluminum and a simpler crystalline structure. Probably, the process of equilibrium phase formation, which competes with dynamic dissolution of aluminides, in experiments on CS of the $Al_{13}Fe_4$ superstructure explains the appearance of aluminide clusters by the cluster short-range ordering or the formation of an amorphous structure [1, 2] according to the microcrystalline model [21].

On the one hand, it is the reduction of the deformation temperature in experiments with the Bridgman anvils that provides a large number of solid solutions and metastable nonstoichiometric aluminides in the form of fore-precipitates and an amorphous structure. On the other hand, a high density of dislocations, which is caused by deformation, gives rise to the competitive precipitation of diffusion-controlled metastable structures in accordance with the phase diagram [9] and the stable Al_5Fe_2 aluminide. It should be noted also that the secondary $Al_{13}Fe_4$ superstructure is not formed in experiments. This is explained by a large number (over 100) of atoms in a unit cell [26] of this compound.

5. Conclusion

Mössbauer spectroscopy examination showed that compression shear of quickly quenched Al–Fe alloys containing 2–5 mass% Fe at 300 K led to dissolution of the metastable Al_5Fe phase, which was followed by the formation of a supersaturated Al–Fe solid solution, the metastable Al_9Fe_2 phase, and defective modifications Al_6Fe(d), Al_9Fe_2(d) and Al_iFe(d). The latter presumably resulted from the saturation of the phases with defects like structural vacancies. The mechanism of dynamic dissolution of the aluminides was realized with a 'subtraction'-type stoichiometry $Al_6Fe + Al \rightarrow Al_{6-x}Fe + Al–Fe + Al$. This was probably connected with a high energy and poor solubility of iron in the aluminum matrix. In other words, a regular feature of mechanically activated phase transformations was in effect, by which the concentration of the less soluble and the less diffusive mobile element increases in the dissolved phase. The defective modification Al_6Fe(d) and metastable Al_9Fe_2 could be formed in the Al–2(5)Fe alloys already during quick quenching. This observation testified to a common vacancy mechanism of phase transformations during quick quenching and intensive plastic deformation.

Stable $Al_{13}Fe_4$ aluminides, which were formed in cast alloys of the compounds at hand, were more stable under CS. Their dissolution involved disordering and the formation of aluminide clusters after the short-range-order cluster type.

Synthesis of mechanical powder mixtures Al–5 mass% ^{57}Fe led to the formation of supersaturated Al–Fe solid solutions and defective modifications analogously to CS

deformation of the quenched alloys, which transformed to metastable Al_9Fe_2 and Al_6Fe aluminides and the stable Al_5Fe_2 aluminide upon annealing.

Deformation-induced Al_6Fe(d) and Al_9Fe_2(d) transformed to the known metastable Al_6Fe and Al_9Fe_2 phases and a stable Al_5Fe_2 phase during low-temperature annealing of both cast alloys and alloys synthesized from mechanical mixtures. The formation of the Al_9Fe_2 and Al_5Fe_2 phases was explained by the competition of the precipitation of phases in the structure saturated with deformation vacancies. The observed deformation-induced phases represented extremely dispersed fore-precipitates or clusters, whose structure could be identified at the local level of nearest atomic neighbors by Mössbauer spectroscopy.

Acknowledgments

This study was supported by the grant 'Fundamental problems of physics and chemistry of nanosized systems and nanomaterials' from the Presidium of the Russian Academy of Sciences.

References

[1] Cardellini F, Contini V, Gupta R, Mazzone G, Montone A, Perin A and Principi G 1998 *J. Mater. Sci.* **33** 2519–27
[2] Fadeeva V I and Leonov A V 1992 *Mater. Sci. Forum* **88–90** 481–8
[3] Forder S D, Brooks J S, Reeder A and Evans P V 1999 *Scr. Metall.* **40** 45–8
[4] Stickels C A and Bush R H 1971 *Metall. Trans.* **2** 2031–42
[5] Preston R S and Gerlach R 1971 *Phys. Rev.* B **3** 1519–26
[6] Preston R S, Nasu S and Gonser U 1979 *J. Physique* **40** (Suppl. 3) C2 564–5
[7] Sassa K, Goto H, Ishida Y and Kato M 1977 *Scr. Metall.* **11** 1029–32
[8] Sassa K, Ishida Y and Kaneko K 1979 *J. Physique* **40** C2 556–88
[9] Young R M K and Clyne T W 1981 *Scr. Metall.* **15** 1211–6
[10] Shabashov V A, Korshunov L G, Mukoseev A G, Sagaradze V V, Makarov A V, Pilyugin V P, Novikov S I and Vildanova N F 2003 *Mater. Sci. Eng.* A **346/1-2** 196–207
[11] Shabashov V A, Litvinov A V, Mukoseev A G, Sagaradze V V, Desyatkov D V, Pilyugin V P, Sagaradze I V and Vildanova N F 2003 *Mater. Sci. Eng.* A **361/1-2** 137–47
[12] Shabashov V A, Mukoseev A G, Sagaradze V V and Litvinov A V 2003 *Izv. Akad. Nauk Ser. Fiz.* **67** 1041–7 (Russian version of *Bull. RAS, Physics*)
[13] Sagaradze V V, Shabashov V A, Lapina T M, Pecherkina N L and Pilyugin V P 1994 *Phys. Met. Metall.* **78** 619–31
[14] Mukoseev A G, Shabashov V A, Sagaradze V V and Sagaradze I V 2001 *Mater. Sci. Eng.* A **316** 174–81
[15] Rusakov V S 1999 *Izv. Akad. Nauk, Ser. Fiz.* **63** 91–8 (Russian version of *Bull. RAS, Physics*)
[16] Nemoshkalenko V V, Rasumov O N and Gorskii V V 1968 *Phys. Status Solidi* **29** 45–8
[17] Stolyarov V V, Soshnikova E P, Brodova I G, Bashlykov D V and Kil'mametov A R 2002 *Fiz. Met. Metalloved.* **93** 74–81
[18] Brodova I G, Bashlykov D B, Shirinkina I G, Yablonskikh T I and Stolyarov V V 2003 *Perspekt. Mater.* (3) 67–72
[19] Brodova I G, Bashlykov D V, Yablonskikh T I and Stolyarov V V 2002 *Phys. Met. Metallogr.* **94** 582–90
[20] Black P J 1955 *Acta Crystallogr.* **8** 175–82
[21] Gaskell P H 1983 Models of amorphous metals structure *Glassy Metals II* (*Springer Topics in Applied Physics* vol 53) ed H Beck and H-J Guntherodt (Berlin: Springer)
[22] Kuznetsov A R and Sagaradze V V 2002 *Phys. Met. Metallogr.* **93** 404–7
[23] Gavrilyuk V S 1987 *Distribution of Carbon in Steel* (Kiev: Naukova Dumka) p 208
[24] Gapontsev V L and Kondratev V V 2002 The problems of nanocrystalline materials *Proceedings (Ekaterinburg, UD RAS)* pp 482–93
[25] Skakov Yu A 2004 *Metalloved. Term. Obrab. Met.* **4** 3–12
[26] Neverov V V and Zhitnikov P P 1996 *Fiz. Met. Metalloved.* **81** 132–6 (Russian version of *Phys. Met. Metall.*)